Small angle X-ray scattering resolves internal composition of *E. coli* cells

A.R. von Gundlach[1], V.M. Garamus[2], T. M. Willey[4], J. Ilavsky[3], K. Hilpert[5*], A. Rosenhahn[1*]

[1] Analytical Chemistry - Biointerfaces, Ruhr-University Bochum, Universitätsstr. 150, 44780 Bochum, Germany.

[2] Helmholtz-Zentrum Geesthacht, Zentrum für Material- und Küstenforschung GmbH, Max-Planck-Straße 1, 21502 Geesthacht, Germany.

[3] X-Ray Science Division, Argonne National Laboratory, 9700 S. Cass Ave., Argonne, IL 60439.

[4] Lawrence Livermore National Laboratory, 7000 East Avenue, Livermore, CA 94550 (USA).

[5] Institute of Infection and Immunity, St. George's University of London (SGUL), Cranmer Terrace, London SW17 0RE, United Kingdom.

** both authors contributed equally*

Abstract

The application of small angle X-ray scattering (SAXS) to whole *Escherichia coli* cells is challenging due to the variety of internal constituents. To resolve their contributions, the outer shape was captured by ultra-small angle X-ray scattering (USAXS) and combined with the internal structure resolves in SAXS. Built on this data, a model for major structural components of *E. coli* was developed. It was possible to deduce information on occupied volume, occurrence and average size of the most important intracellular constituents: ribosomes, DNA, and proteins. We studied *E. coli* after treatment with three different antibiotic agents: chloramphenicol, tetracycline and rifampicin and monitored the impact on the intracellular constituents.

Keywords: small angle X-ray scattering, ultra small angle scattering, transmission electron microscopy, ultrastructure of E. coli, antibiotics, ribosomes, nucleoid, SAXS, USAXS.

Introduction

A broad variety of nanoscale imaging techniques has been established to study the intracellular organization of bacteria. Methods include imaging of thin sections with electron microscopy[1], high-resolution fluorescence light microscopy[2], and whole cell imaging with X-ray microscopy.[3] For biological samples, such as bacteria, a large number of cells need to be imaged to obtain statistically significant sampling of the population, which is labor intensive and limited in throughput. Scattering techniques have the general advantage of providing data averaged over a large number of samples (millions of entities) using only seconds of exposure time. Suspensions of the samples can be used without any preprocessing, however, the technique provides only occurrence of specific size ranges instead of real space images. Nonetheless, small angle X-ray scattering has matured during the past decade and many synchrotron facilities around the globe provide high-throughput operation and automated analysis pipelines.[4] A major application of SAXS is to study shape[5,6] and function[7] of hydrated proteins. Besides it has been applied to understand the organization of soft organic matter like hydrated membranes[8], micelles[9], human bone tissue[10], human breast cancer tissue[11], and melanosomes[12].

Application of SAXS to complex systems such as entire cells requires specialized data analysis and the correlation with other structural sensitive methods such as microscopy. We showed recently that the morphological fingerprint of bacteria provided by standard SAXS ($q \sim 0.01\ nm^{-1} – 4\ nm^{-1}$) is a powerful marker for antibiotic modes of action[13]. Due to the complexity of the system (whole bacterial cells) and the limited q-range, a principle component analysis was used to classify the changes in the bacterial ultrastructure recorded with SAXS. The correlation with transmission electron microscopy suggested that the distribution of DNA located in the bacterial nucleoid contributed majorly to the changes observed in the SAXS signal.

In the present study we acquired scattering data across a large q-range ($0.002 – 3.5\ nm^{-1}$) covering the outer dimensions of *Escherichia coli* and developed a model to analyze the obtained scattering curves. The simplified model considers different intracellular objects, on the length scale of ribosomes, DNA, and proteins. Structural changes after the addition of antibiotics were determined and analyzed by this new model. We selected inhibitors of the protein synthesis (tetracycline and chloramphenicol) and an inhibitor of the RNA-synthesis since they are expected to change the internal composition of a cell.

Material and Methods

Sample Preparation

Escherichia coli (K12, wild type, DSM 498, ATCC 23716) from overnight cultures were diluted in Mueller-Hinton broth (1:40) and incubated at 37°C until an optical density (OD_{600}) of 0.45 was reached. This culture is in the exponential growth phase and has approx. 10^8 cells ml^{-1}. The antibiotic (chloramphenicol (60 µg ml^{-1}), tetracycline (30 µg ml^{-1}) and rifampicin (100 µg ml^{-1})) were added to 1 ml of inoculum each and incubated for 4 hours at 37° C. After centrifugation, the bacterial pellets were washed with PIPES buffer (0.1 M, pH = 7.0), and fixed in a 2.5 % glutaraldehyde solution in PIPES buffer. To remove the fixative, the samples were washed three times in a PBS buffer (10 mM, pH = 7.0) and stored at 4° C. The final sample volume was 100 µl.

Small angle X-ray scattering

The SAXS experiments were performed at the P12 BioSAXS beamline at PETRA III (EMBL/DESY) in Hamburg, Germany. The beamline delivers photons with an energy of 12.8 keV to a spot size of 0.2 mm × 0.1 mm with a flux of 1 x 10^{13} s^{-1}. The diffraction patterns were collected with a Pilatus 2M detector (Dectris, Switzerland). A sample robot changer was employed to collect the diffraction patterns. The 20 µL of cell suspension automatically was delivered by sample robot into a glass capillary (20° C) and the illuminated volume contained roughly 10^6 fixed *E. coli* cells. In order to obtain a homogeneous suspension, the samples were resuspended with a pipet prior to the measurements. 20 diffraction patterns were collected for every sample, each with an exposure time of 0.05 s. The PBS buffer was measured before and after every measurement and the average of both was used as background subtracted from the sample curve. To avoid radiation damage by subsequent illuminations curves showing deviations were discarded by the automated data acquisition software[14]. The instrument was calibrated using silver behenate and the observed q-range was 0.01 nm^{-1} to 4 nm^{-1}.[15]

Ultra-small angle X-ray scattering

Ultra-small angle X-ray scattering experiments were performed on the USAXS instrument at 15ID beamline (now located at the 9ID) at the Advanced Photon Source, Argonne National Laboratory in Argonne, USA. The beam size was 1 mm × 2 mm with a photon flux of 10^{13} Ph/s and a photon energy of 17 keV. This Bonse-Hart camera[16] was operated in slit smeared configuration with Si(220) collimator and analyzer crystals; a Si photodiode was used for detection.[17] The observed q-range was 1.6 × 10^{-3} nm^{-1} to 0.12 nm^{-1}. The samples were delivered in suspension in PCR-tubes with a cell density of approx. 10^{10} ml^{-1}. The beam was centered optically on each sample. The

USAXS-data was processed with the INDRA data reduction package for Igor Pro® (Wavemetrics, Portland, USA).[16]

Data analysis

Inhomogeneities in the electron density are the origin of the scattering signal *I*(*q*) recorded in SAXS. The scattering vector *q* is calculated as $q = \frac{4\pi}{\lambda}\sin(\theta)$, where λ is the X-ray wavelength and θ is half of the scattering angle. Inhomogeneities in the electron density are modelled as solid particles with homogeneous density For multiple populations of particles with known shapes the scattering signal *I*(*q*) can be modelled using suitable scattering form factors *F(q, r)*[18,19]:

$$I(q) = \int |\Delta\rho|^2 S_k(q) \int F(q,r)^2 V(r) f_k(r) dr$$

Here $|\Delta\rho|^2$ is the scattering contrast, $S_k(q)$ accounts for interactions between particles, and *V(r)* is the volume of a single particle. Polydisperse solutions can be described by the volume size distribution *f(r),* which describes the volume occupied by particles of a certain size. All these contributions are functions of the radius of a scatterer *r* and the scattering vector *q*. The volume size distribution *f*(*r*) is related to the number size distribution *N*(*r*) by:

$$f(r) = V(r)N(r) = V(r)N_T\,\Psi(r)$$

where N_T is the total number of scatterers and $\Psi(r)$ the probability of occurrence of a scatterer at a radius *r*. The data analysis was carried out with the "Modelling II" package of the *IRENA* macros[19] for Igor Pro® (Wavemetrics Inc., Portland, USA). As a first approximation to model the internal cellular particles, the structure factor $S_k(q)$ was set to 1 i.e., there is no interaction between components.

Merging of datasets

In the experiments, untreated *E. coli* and *E. coli* treated with choramphenicol, tetracycline or rifampicin were investigated. The curves for *E. coli* treated with chloramphenicol measured at BioSAXS and USAXS had an overlapping *q*-interval between 0.005 nm^{-1} and 0.01 nm^{-1} which was used for adjusting the relative intensities (Fig. S1). In the other cases, the noise level in the USAXS experiments limited the q-range. Thus the outer shape of the bacterial cell was modeled as a homogeneous cylinder (Table S1). The model was extrapolated to the BioSAXS data and allowed to scale the relative intensities (Fig. S2).

Results

E. coli has usually a length of ≈ 2 µm and a diameter of ≈ 500 nm. The enclosed intracellular components contain small entities, such as proteins or ribosomes which are on the scale of a few nanometers. The challenge in investigating bacteria with scattering techniques is that a large q-range is required if all size ranges from small proteins (few nm) up to the diameter of the bacteria are meant to be recorded. Most SAXS experiments at both, laboratory and synchrotron sources, are optimized for proteins and therefore size ranges of one to one hundred nanometers are accessible. For covering the problem of the large outer size of *E. coli* one needs to cover size ranges up to 5 µm which is only possible if scattering at small angles is recorded using a ultra-small angle scattering instruments. In this study we recorded the internal nanoscale information (1 nm – 120 nm) at the BioSAXS instrument (P12, Petra III, EMBL/DESY, Hamburg, Germany) and combined it with USAXS data (100 nm - 3 µm) recorded at the USAXS instrument (APS, Argonne, USA). The difference in photon energy (12.8 keV at BioSAXS and 17 keV at USAXS) and the resulting difference in scattering contrast $|\Delta\rho|^2$ of a whole *E. coli* cell (The best fit to model t0.65695 × 10^{20} cm^4 at 12.8 keV and 0.65706 × 10^{20} cm^4 at 17 keV) is very small and was neglected for modeling.

The best fit to model the outer shape of untreated *E. coli* was a homogeneous cylinder with a radius of 418 ± 40 nm and an aspect ratio of 2 (Fig. S2, Table S1). Using the approximated values for the scattering contrast, the internal components of *E. coli* were modeled as filled spheres, the simplest geometrical shape. During fitting the data it became clear that in addition to the outer shape, a minimum of three populations of scatterers are needed to be modeled to match the ‘shoulders’ in the experimental SAXS curves of the bacterial cells (Fig. 1). When representing the internal constituents with two populations no fit of the curve could be obtained whereas four populations resulted in an undefined model. The mean radius of the three internal populations matched the sizes of three important intracellular components of *E. coli*. The smallest size had a mean diameter of 3.4 nm. This diameter fits well to the size range of many proteins which have an average diameter of 2 nm - 5 nm[20,21]. The second population had an average diameter of 9 nm. This value is close to the typical diameters of three intertwined DNA fibers complexed with histone-like proteins (10 nm).[22,23] The mean diameter of the third population was determined to be 26 nm, which is close to the typical diameter of ribosomes (diameter in crystal structure: 21 nm[24]). These three normal distributed structural populations are enclosed in the cell wall of the bacterium, modeled as a cylindrical shape resulted in an aspect ratio of 2 and a diameter of 840 nm.

To account for differences in the electron density of internal components and the whole bacterial cell, and the respective scattering contrasts were approximated. From literature data on the elemental composition and reported densities, the scattering contrast of proteins, DNA, and ribosomes was calculated (Table 1). For the whole bacterial cell, the average density was calculated from the dry mass composition of *E. coli*[24] and its water content[25]. This leads to a more accurate description of the internal components and the relative volume they occupy. For comparison a model with all scattering contrasts $|\Delta\rho|^2 = 1$ was calculated and is depicted as dotted line in figure 1b-c.

Component	**Density (g/ml)**	**Approximated element composition**	**Scattering contrast in H_2O $\|\Delta\rho\|^2$**
Proteins	1.35 [25]	$NC_5O_2H_8$	7.983×10^{20} cm^{-4}
DNA	2 [26]	$PN_5O_7C_{10}H_{14}$	30.64×10^{20} cm^{-4}
Ribosomes	1.62 [27]	$PN_5O_8C_{10}H_{14}$	23.70×10^{20} cm^{-4}
***E. coli* cell**	1.1 [28]	$C_{0.09}H_{0.61}O_{0.27}N_{0.019}$ [28,29]	0.665×10^{20} cm^{-4}

Table 1: Approximation of the scattering contrasts at 12.8 keV derived from literature data on elementary composition and density. The density of a whole bacterial cell was calculated from the dry mass composition[28] and the water content[29]. The elementary composition of DNA and ribosomes were calculated from their structure. All contrasts are given relative to H_2O. (Density: 1 g/ml, $|\Delta\rho|^2$ to vacuum: 88.73×10^{20} cm^{-4}). The calculations were performed using the scattering contrast module of the *IRENA* macros[19] for Igor Pro®.

The model best matching the experimental data including approximated scattering contrasts provides a distribution of volumes (Fig. 1b) and their occurrence (Fig. 1c). These values were normalized to yield information per single *E. coli* cell. Therefore the volume / occurrence of internal constituents (populations 1-3 in Fig. 1) were normalized to the volume / occurrence of the outer cell (population 4 in Fig. 1). The given number and percentages are always for the average size of a population.

Especially for DNA-histone complexes and ribosomes, the number and volume estimations are considerably close to literature values. The volume content of DNA per cell is 17.2 %, fitting well to volume estimations of the bacterial nucleoid of 20% obtained by fluorescence microscopy[30]. The same is true for the estimated number of ribosomes which is with 9900 per cell close to the literature value for *E. coli* of 18600 per cell[29]. The number of proteins seems to be overestimated in our data analysis with 8×10^8 proteins (average diameter of 3.5 nm) per cell compared to calculations based on protein content of dry mass yielding 2.5×10^6 proteins per *E. coli* cell[29]. This systematic overestimation could be a consequence of the fact that the first solvation shell around

every molecule contribute to the SAXS signal[31] thus exaggerating the volume relative to dry mass analysis. Additionally this population includes a size range of ~ 4 nm to 1.5 nm in diameter which is predominantly proteins but also includes other cellular constituents such as cell wall components, mRNA and extracellular proteins which may be attached during the fixation step. Considering the simplicity of this model, the obtained volumes and numbers of all populations are surprisingly accurate and the approach can be considered to be complementary to existing methods for determination of the internal composition of bacteria.

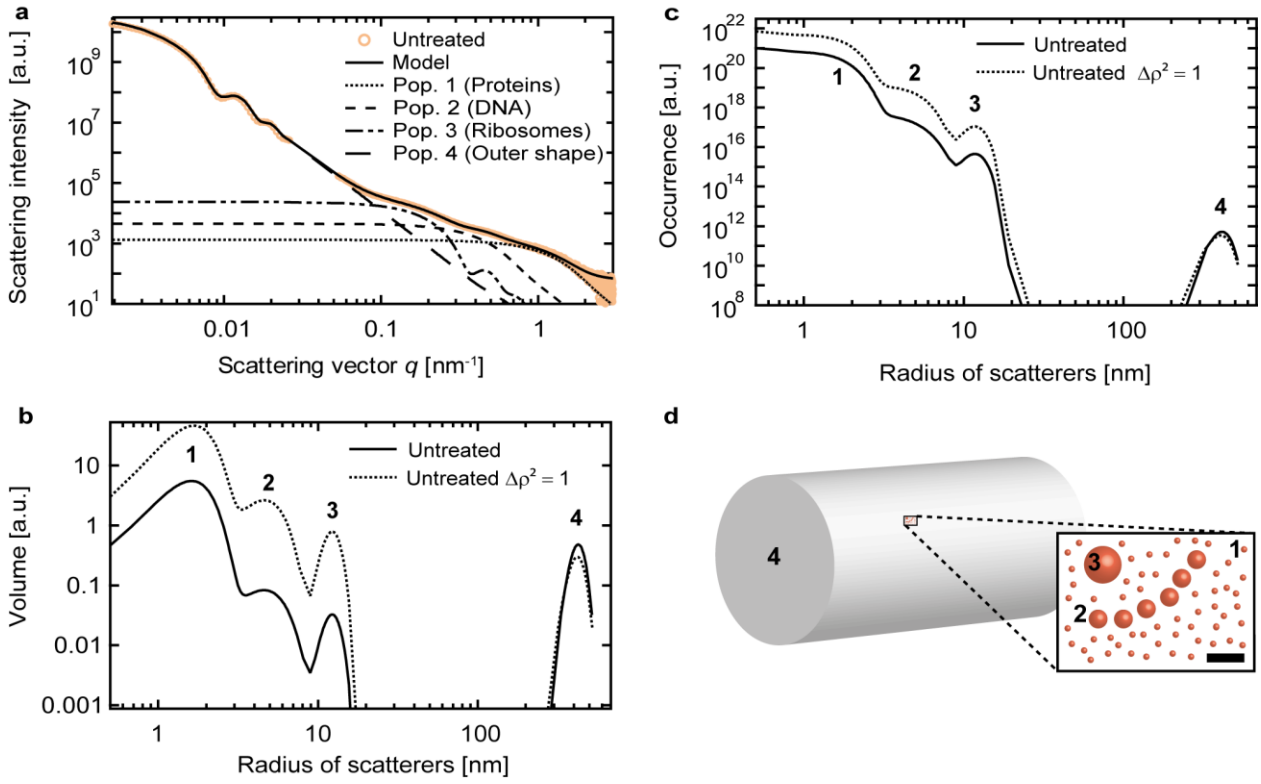

Figure 1: Simplified model for the merged scattering curves of untreated *E. coli* cells. The scattering curves were measured at BioSAXS (12.8 keV, PETRA III, Hamburg, Germany) and USAXS (17 keV, APS, Argonne, USA). a) Model of untreated *E.* coli using four populations of scatterers. The sizes of the scatterers match the sizes of major cellular components (proteins, DNA, and ribosomes) and the outer shape. The outer shape was approximated as cylinder with fixed aspect ratio and the internal components as spheres. b) Volume distribution *f(r)* of the cellular components as function of their radius. The solid line shows the volume distributions adjusted for the scattering contrasts (Table 1), the dotted line assumes $|\Delta\rho|^2 = 1$ for all scatterers. c) Number distribution *N(r)* shows the occurrence of scatterers as a function of their radius. Again the solid line is adjusted for the scattering contrasts (Table 1) and the dotted line assumes $|\Delta\rho|^2 = 1$ for all scatterers. d) Illustration of the model featuring a cylinder representing the outer bacterial shape and the major cellular components as spheres. The scale bar has a length of 20 nm.

Antibiotic treatment

In many cases the bacterial ultrastructure is changed after treatment with antibiotics. We explored how the size and occurrence of the cellular components identified above was affected by incubation with three clinically relevant antibiotics: chloramphenicol, tetracycline, and rifampicin. Chloramphenicol is a protein synthesis inhibitor which prevents the formation of new peptide bonds and associates with the 50S ribosomal subunit.[32] Tetracycline is a protein synthesis inhibitor which binds to the 30S subunit of the ribosome and prevents the binding of a new tRNA molecule by steric interaction.[32] Rifampicin is an RNA synthesis inhibitor which associates with the bacterial RNA polymerase and blocks the path of the elongating RNA chain by steric interaction.[33] After treatment with the different antibiotics at 10x the minimal inhibitory concentration, bacterial suspensions were investigated by SAXS and USAXS and the obtained scattering data was analyzed in the same way as discussed above. Figure 2a shows the impact of antibiotics on the average diameter of intracellular components and the volume occupied by them.

A treatment with tetracycline had no influence on the mean diameter of proteins. Also the cellular volume occupied by proteins remained constant. After treatment the volume occupied by DNA was reduced by 50 %. At the same time, the average radius of three aggregated DNA fibers complexed with histone-like proteins was reduced by 30%. The impact on the ribosomes was smaller, here the occupied volume was found to increase by 20 % while the average radius of a ribosome decreased by 10 %.

These changes were similar after chloramphenicol treatment where protein radius and volume contribution remained unchanged, but the volume of the DNA was reduced by 50 %. The average radius of the ribosomes was also reduced by 10 %. The strong reduction in the volume of the DNA after a tetracycline or chloramphenicol treatment is illustrated by TEM images which reveal the condensation of the DNA in center of the bacterial cell (Fig. 2e).

The SAXS signal of an *E. coli* treated with rifampicin showed an increase of the average radius of three aggregated DNA fibers complexed with histone-like proteins by 20%. The volume occupied by the aggregated DNA remained constant. At the same time, the volume of ribosomes increased by 10 % while retaining the size of an individual ribosome. The size and volume of proteins remained unchanged. TEM images of rifampicin treated *E. coli* feature an expanded nucleoid (Fig. 2e).

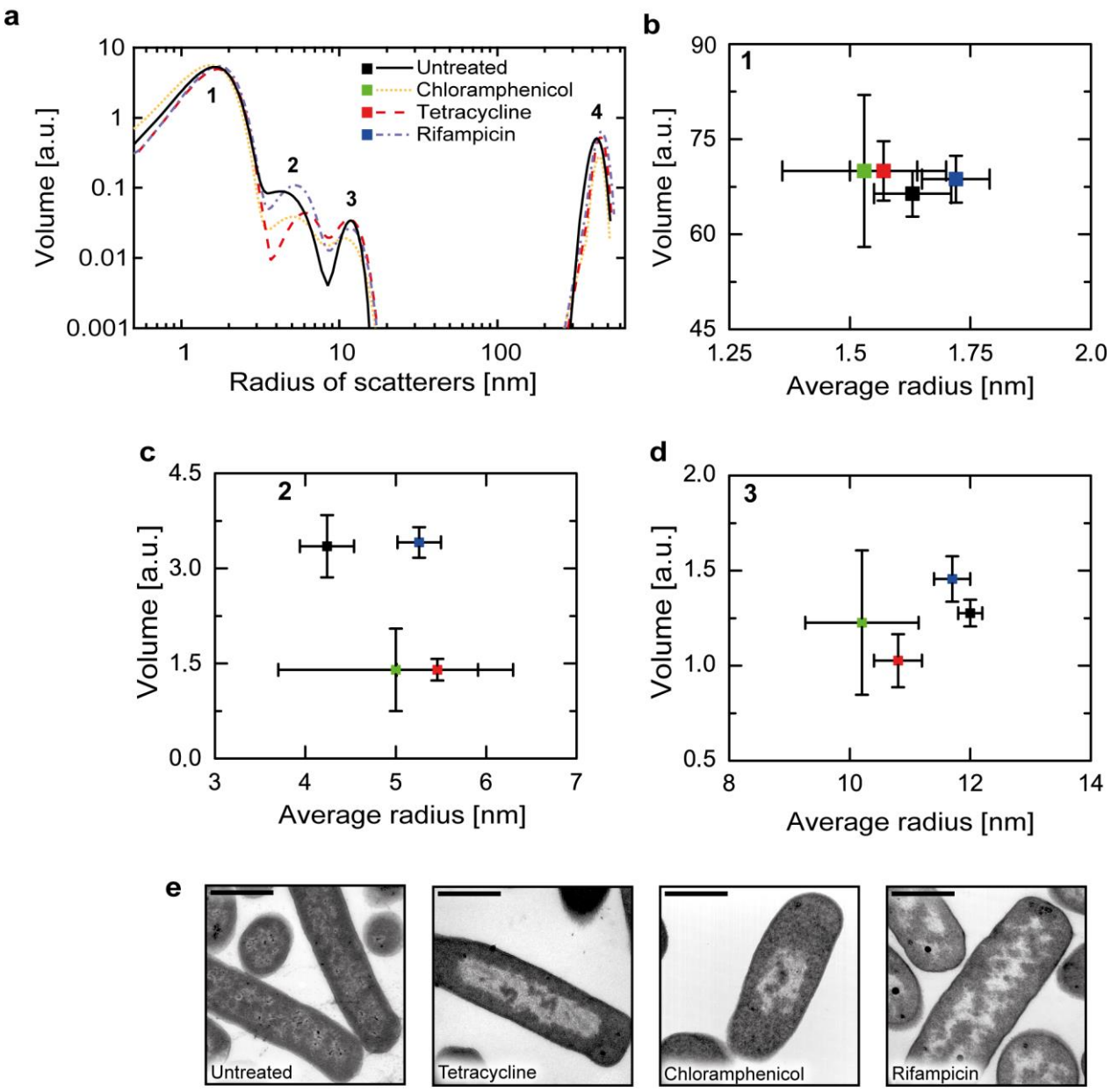

Figure 2: Cellular composition of *E. coli* cells after antibiotic treatment determined by SAXS. a) Volume distribution of the cellular components before and after antibiotic treatment as function scatterers' radius. The total volume and the average radius of each scattering population was extracted from this distribution. b) Average radius and volume of population 1 corresponding to the sizerange of proteins. c) Average radius and volume content of population 2 corresponding to three aggregated DNA fibers covered with histone-like proteins. d) Average radius and volume of population 3 corresponding to ribosomes. The displayed errors bars (b-d) denote the standard deviation of the model from the experimental data calculated with the uncertainty module of the IRENA toolbox. e) Transmission electron micrographs of *E. coli* after antibiotic treatment. The scale has a length of 1 µm.

Discussion

The morphological impact of the antibiotics tetracycline, chloramphenicol and rifampicin on the shape of the bacterial DNA, the so-called nucleoid is well documented in literature: chloramphenicol and tetracycline condense the nucleoid whereas rifampicin leads to an expansion of the nucleoid[34]. The shape of the nucleoid is the result of competing expanding and compacting forces[35]. A major expanding force is 'transertion', which describes the transcription, translation, and insertion of membrane proteins into the cytoplasmic membrane. Since this process occurs in close proximity to the cytoplasmic membrane, it anchors the transcribed bacterial nucleoid onto the cytoplasmic membrane[36]. The suggested compacting forces include DNA binding of proteins, DNA supercoiling, macromolecular crowding and entropy driven depletion attraction. Cabrera et al.[34] suggest that ongoing transcription is necessary for the chloramphenicol-induced nucleoid compaction. In their fluorescence microscopy observations a chloramphenicol treatment condensed the nucleoid and a subsequent rifampicin treatment led to complete expansion of the nucleoid.

The TEM images (Fig. 2e) support this notion as chloramphenicol and tetracycline led to a condensation of the nucleoid while rifampicin facilitated its expansion. In SAXS, chloramphenicol and tetracycline treatments induced a reduction of the overall volume occupied by DNA as suggested by TEM imagery and fluorescence microscopy[37]. The aggregated DNA fibers increase in radius may be a consequence of stress response where sigma factors attach to the DNA (Fig. 2a-d).

While the morphological effect on the DNA is well studied, the effect on the ribosomes has not yet been described. SAXS reveals a reduction in size of the individual ribosome after a treatment with chloramphenicol or tetracycline (Fig. 2) which is most probably a consequence of the segregation of ribosomes and DNA[2] and the removal of freshly synthesized proteins from the close proximity of the ribosomes. The volume occupied by ribosomes is also reduced which suggests that an inhibition of the protein synthesis has a reduction of the total number of ribosomes as a consequence.

A treatment with rifampicin has weaker morphological consequences to the bacterial nucleoid. Here, the inhibition of transcription removes the compacting force and the nucleoid expands.[38] TEM images confirm this effect (Fig. 2e). In SAXS we observed that the volume occupied by the DNA remains constant. Simultaneously we find that the mean radius of the individual DNA fiber increased. We attribute this to a fiber relaxation as consequence of a reduced coiling force. The size and volume of ribosomes remain unchanged.

Summarizing, this work illustrates that SAXS can be used as a structure sensitive tool to gain information on the internal organization of *E. coli* cells on the nanoscale. The measurement of very low scattering angles allowed deconvolution of the contributions of bacterial outer shape and internal constituents. Inside the bacterial cell, the volume content of DNA and the number and volume of ribosomes can be deduced using a simple model. There are no indications for the occurrence of additional scattering contributions from larger, aggregated mesostructures, such as the bacterial nucleoid. Despite the good fit of the data we have to point out that the applied model is limited since only isolated particles are considered, neglecting any interactions. As intrinsic electron densities were used as contrasting markers, no stains and, apart from incubation and fixation, no preprocessing was required for the experiment. This reduced the effort for sample preparation to a minimum and maximizes the achievable sample throughput. Especially the fact that information averaged over millions of cells can be obtained in seconds makes the method particularly interesting for incorporation into the developmental and testing pipeline for novel antimicrobial compounds.

Acknowledgements

The excellent support of Dr. Clement Blanchet (EMBL) and the staff of PETRA III during SAXS measurements is kindly acknowledged. We thank Maria McGlynn and Raymond Moss for the preparation of the TEM samples and the help during the measurements. We acknowledge funding by the Virtual Institute VH-VI-403 (Helmholtz-Society) and the Cluster of Excellence RESOLV (EXC 1069, DFG), startup funding from the Institute of Infection and Immunity and funding from the enterprise office of SGUL. ChemMatCARS Sector 15 is principally supported by the Divisions of Chemistry (CHE) and Materials Research (DMR), National Science Foundation, under grant number NSF/CHE-1346572. Use of the Advanced Photon Source, an Office of Science User Facility operated for the U.S. Department of Energy (DOE) Office of Science by Argonne National Laboratory, was supported by the U.S. DOE under Contract No. DE-AC02-06CH11357.

Author contributions

Conceived and designed the experiments: AR, KH, ARVG. Performed the experiments: ARVG, VMG, TMW, JI. Analyzed and interpreted the data: ARVG, AR. Wrote the manuscript: ARVG, AR.

References

1. Matias, V. R. F., Al-Amoudi, A., Dubochet, J. & Beveridge, T. J. Cryo-Transmission Electron Microscopy of Frozen-Hydrated Sections of Escherichia coli and Pseudomonas

aeruginosa. *J. Bacteriol.* **185,** 6112–6118 (2003).

2. Bakshi, S., Siryaporn, A., Goulian, M. & Weisshaar, J. C. Superresolution imaging of ribosomes and RNA polymerase in live Escherichia coli cells. *Mol. Microbiol.* **85,** 21–38 (2012).

3. Schneider, G. *et al.* Three-dimensional cellular ultrastructure resolved by X-ray microscopy. *Nat. Methods* **7,** 985–7 (2010).

4. Graewert, M. A. & Svergun, D. I. Impact and progress in small and wide angle X-ray scattering (SAXS and WAXS). *Curr. Opin. Struct. Biol.* **23,** 748–54 (2013).

5. Blanchet, C. E. & Svergun, D. I. Small-angle X-ray Scattering on Biological Macromolecules and Nanocomposites in Solution. *Annu. Rev. Phys. Chem.* **64,** 37–54 (2013).

6. Wright, K. E. *et al.* Structure of malaria invasion protein RH5 with erythrocyte basigin and blocking antibodies. *Nature* **515,** 427–429 (2014).

7. Fang, X. *et al.* An unusual topological structure of the HIV-1 Rev response element. *Cell* **155,** 594–605 (2013).

8. Mendil-Jakani, H., Zamanillo Lopez, I., Legrand, P. M., Mareau, V. H. & Gonon, L. A new interpretation of SAXS peaks in sulfonated poly(ether ether ketone) (sPEEK) membranes for fuel cells. *Phys. Chem. Chem. Phys.* **16,** 11243–50 (2014).

9. Filippov, S. K. *et al.* Hydrolytically degradable polymer micelles for drug delivery: a SAXS/SANS kinetic study. *Biomacromolecules* **14,** 4061–70 (2013).

10. Granke, M. *et al.* Microfibril orientation dominates the microelastic properties of human bone tissue at the lamellar length scale. *PLoS One* **8,** e58043 (2013).

11. Conceição, a. L. C., Antoniassi, M., Geraldelli, W. & Poletti, M. E. Mapping transitions between healthy and pathological lesions in human breast tissues by diffraction enhanced imaging computed tomography (DEI-CT) and small angle x-ray scattering (SAXS). *Radiat. Phys. Chem.* **95,** 313–316 (2014).

12. Gorniak, T. *et al.* Nano-scale morphology of melanosomes revealed by small-angle X-ray scattering. *PLoS One* **9,** e90884 (2014).

13. von Gundlach, A. R. *et al.* High throughput method to classify the mode of action of novel antimicrobial compounds. Biochimica et Biophysica Acta (BBA) - Biomembranes, (2016)

doi:10.1016/j.bbamem.2015.12.022.

14. Franke, D., Kikhney, A. G. & Svergun, D. I. Automated acquisition and analysis of small angle X-ray scattering data. *Nucl. Instruments Methods Phys. Res. A* **689,** 52–59 (2012).

15. Blanton, T. N., Barnes, C. L. & Lelental, M. Preparation of silver behenate coatings to provide low- to mid-angle diffraction calibration. *J. Appl. Crystallogr.* **33,** 172–173 (2000).

16. Ilavsky, J. *et al.* Ultra-small-angle X-ray scattering at the Advanced Photon Source. *J. Appl. Crystallogr.* **42,** 469–479 (2009).

17. Ilavsky, J. *et al.* Ultra-Small-Angle X-ray Scattering Instrument at the Advanced Photon Source: History, Recent Development, and Current Status. *Metall. Mater. Trans. A* **44,** 68–76 (2013).

18. Glatter, O. & Kratky, O. *Small Angle X-ray Scattering*. (Academic Press, 1982). at <https://books.google.de/books?id=J8fvAAAAMAAJ>

19. Ilavsky, J. & Jemian, P. R. Irena : tool suite for modeling and analysis of small-angle scattering. *J. Appl. Crystallogr.* **42,** 347–353 (2009).

20. Erickson, H. P. Size and shape of protein molecules at the nanometer level determined by sedimentation, gel filtration, and electron microscopy. *Biol. Proced. Online* **11,** 32–51 (2009).

21. Skovgaard, M., Jensen, L. J., Brunak, S., Ussery, D. & Krogh, A. On the total number of genes and their length distribution in complete microbial genomes. *Trends Genet.* **17,** 425–428 (2001).

22. Ohniwa, R. L. *et al.* Transcription-coupled nucleoid architecture in bacteria. *Genes to Cells* **12,** 1141–52 (2007).

23. Kim, J. *et al.* Fundamental structural units of the Escherichia coli nucleoid revealed by atomic force microscopy. *Nucleic Acids Res.* **32,** 1982–92 (2004).

24. Schuwirth, B. S. *et al.* Structures of the bacterial ribosome at 3.5 A resolution. *Science (80-.).* **310,** 827–834 (2005).

25. Fischer, H., Polikarpov, I. & Craievich, A. F. Average protein density is a molecular-weight-dependent function. *Protein Sci.* **13,** 2825–2828 (2004).

26. Feijó Delgado, F. *et al.* Intracellular Water Exchange for Measuring the Dry Mass, Water Mass and Changes in Chemical Composition of Living Cells. *PLoS One* **8,** e67590 (2013).

27. Fenwick, M. L. The density of ribosomes bearing messenger RNA in phage-infected and normal bacteria. *J. Cell Sci.* **8,** 649–658 (1971).

28. Duboc, P., Marison, I. & von Stockar, U. *Handbook of Thermal Analysis and Calorimetry*. (Elsevier Science, 1999).

29. Neidhardt, F. C. & Curtiss, R. *Escherichia Coli and Salmonella: Cellular and Molecular Biology*. (ASM Press, 1996). at <http://books.google.de/books?id=FW0eqAAACAAJ>

30. Birge, E. A. *Bacterial and Bacteriophage Genetics*. (Springer, 2006). at <https://books.google.de/books?id=_Q5bSAv2-KoC>

31. Chen, P. & Hub, J. S. Validating Solution Ensembles from Molecular Dynamics Simulation by Wide-Angle X-ray Scattering Data. *Biophys. J.* **107,** 435–447 (2014).

32. Wilson, D. N. The A-Z of bacterial translation inhibitors. *Crit. Rev. Biochem. Mol. Biol.* **44,** 393–433 (2009).

33. Campbell, E. A. *et al.* Structural Mechanism for Rifampicin Inhibition of Bacterial RNA Polymerase. *Cell* **104,** 901–12 (2001).

34. Chai, Q. *et al.* Organization of ribosomes and nucleoids in Escherichia coli cells during growth and in quiescence. *J. Biol. Chem.* **289,** 11342–52 (2014).

35. Cabrera, J. E., Cagliero, C., Quan, S., Squires, C. L. & Jin, D. J. Active transcription of rRNA operons condenses the nucleoid in Escherichia coli: examining the effect of transcription on nucleoid structure in the absence of transertion. *J. Bacteriol.* **191,** 4180–5 (2009).

36. Woldringh, C. L. The role of co-transcriptional translation and protein translocation (transertion) in bacterial chromosome segregation. *Mol. Microbiol.* **45,** 17–29 (2002).

37. Jin, D. J., Cagliero, C. & Zhou, Y. N. Role of RNA polymerase and transcription in the organization of the bacterial nucleoid. *Chem. Rev.* **113,** 8662–82 (2013).

38. Weng, X. & Xiao, J. Spatial organization of transcription in bacterial cells. *Trends Genet.* **30,** 287–297 (2014).

Supplementary Information

Merging USAXS and SAXS datasets

Since the differences in photon energies have only very little influence on the scattering contrast their impact was neglected. The dataset of chloramphenicol treated *E. coli* featured an overlapping section with identical slope which allowed to adjust the relative intensities (Fig. S1). The different in photon energies were neglected as the scattering contrast is very similar ($|\Delta\boldsymbol{\rho}|^2$ of a whole *E. coli* cell ($\boldsymbol{\rho}$ = 1.1 g ml^{-1}, $C_{0.09}H_{0.61}O_{0.27}N_{0.019}$) is 0.65695 × 10^{20} cm^4 at 12.8 keV and 0.65706 × 10^{20} cm^4 at 17 keV).

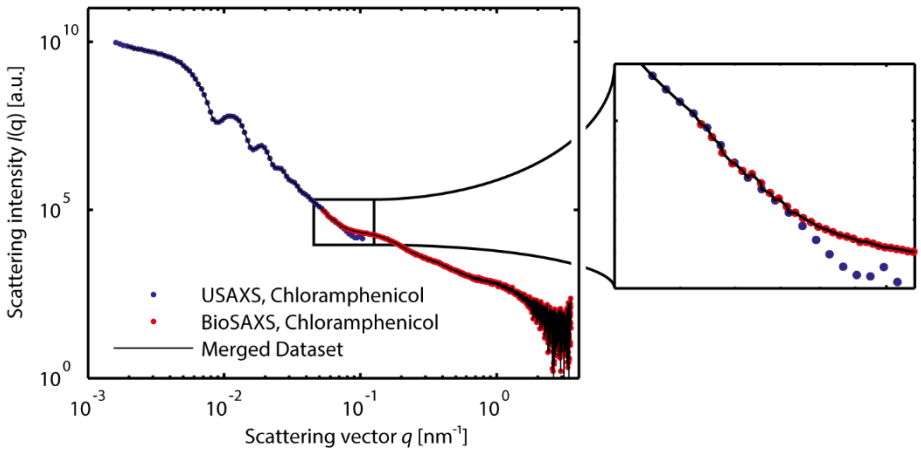

Supplementary figure S1: SAXS curve of chloramphenicol treated, fixed *E. coli* measured at the USAXS (17 keV, APS, Argonne, USA) and the BioSAXS (12.8 keV, PETRA III, Hamburg, Germany). Both datasets show an overlapping section within which both feature the same slope. This overlap allows to scale their relative intensities.

The intensity of the USAXS signal varied with sample density. Thus, the usable q-range which was clearly separated from the noise level was different for each batch of analyzed samples. Only in some cases, the USAXS q-range overlapped with the one of the BioSAXS experiments. The correct relative intensities were found by modelling the scattering of the outer bacterial shape as cylindrical and then extrapolated to the q-range covered in the BioSAXS experiments.

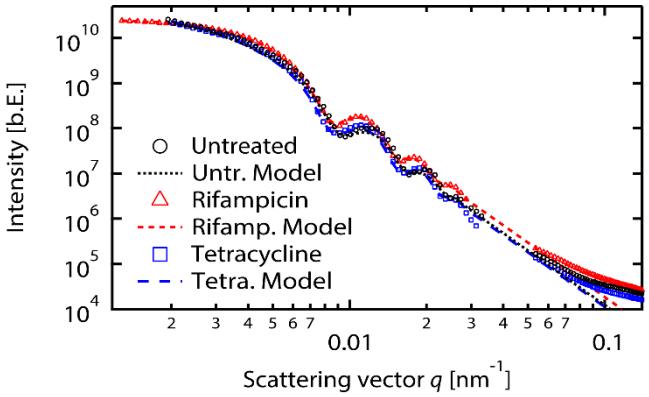

Supplementary figure S2: Merging of the scattering data from USAXS and BioSAXS. The scattering data of the USAXS and BioSAXS did not overlap for the untreated bacterial cells (black) and treatments with rifampicin (red) and tetracycline (blue). Thus the outer shape of the bacterial cell was modeled as a homogeneous cylinder with fixed aspect ratio (Model). The model was extrapolated to the BioSAXS data and allowed to scale the relative intensities. The overlap of the chloramphenicol treated bacterial cells is shown in Figure S1.

A population of normal distributed cyclinders with a constant aspect ratio was found to represent the scattering data of the outer shape in USAXS best. The resulting information is the aspect ratio of the model cylinder, its average radius and standard deviation (width of the distribution). For comparison we quantified the dimensions of bacterial cells in the TEM images, which alwalys display single sections through the bacterial cells. We measured ~ 14 individual cells per treatememt. The comparison indicates, that our USAXS analysis seems to underestimate the aspect ratio.

Antibiotic	Aspect ratio cylinder (USAXS)	Average radius *R* [nm] (USAXS)	Std. dev. *σ* [nm] (USAXS)	Aspect ratio TEM	Radius TEM [nm]
Untreated	2	418 ± 10	40 ± 10	3,7 ± 0,8	450 ± 40
Chloramphenicol	1	441 ± 10	32 ± 10	2,6 ± 0,6	550 ± 70
Tetracycline	2	450 ± 10	34 ± 10	3,2 ± 0,7	550 ±70
Rifampicin	1	455 ± 10	40 ± 10	3,2 ± 1,2	600 ± 60

Table S1: Data for the modelling of the outer shape of the bacterial cell as homogeneous cylinders with fixed aspect ratio. The standard deviation around the average radius of the population (normal distribution) indicates the monodispersity.